JOURNAL OF GEOPHYSICAL RESEARCH, VOL. 98, NO. D9, PAGES 16,893–16,908, SEPTEMBER 20, 1993

Third Soviet-American Gases and Aerosols (SAGA 3) Experiment: Overview and Meteorological and Oceanographic Conditions

J. E. JOHNSON,[1,2] V. M. KOROPALOV,[3] K. E. PICKERING,[4] A. M. THOMPSON,[5] N. BOND,[1,2] AND J. W. ELKINS[6]

The primary goal of the third joint Soviet-American Gases and Aerosols (SAGA 3) experiment was to study trace gases and aerosols in the remote marine boundary layer. SAGA 3/leg 1 took place from February 13 to March 13, 1990, aboard the former Soviet R/V *Akademik Korolev* and consisted of five equatorial transects (designated transects 1 through 5) between 15°N and 10°S on a cruise track from Hilo, Hawaii, to Pago-Pago, American Samoa. Specific objectives were to study (1) the oceanic distribution and air-sea exchange of biogenic trace gases; (2) photochemical cycles of C-, S-, and N-containing gases in the marine boundary layer; (3) the distribution of aerosol particles in the marine boundary layer and their physical and chemical properties; (4) interhemispheric gradients and latitudinal mixing of trace gases and aerosols; and (5) stratospheric aerosol layers. SAGA 3/leg 2 continued from March 17 to April 7, 1990, with one more equatorial transect between American Samoa and the northern coast of the Philippines (transect 6) followed by a final transect to Singapore (transect 7). During leg 2, most former Soviet measurements continued, but with the exception of measurements of nitrous oxide (N_2O) and selected halocarbons in the air and surface waters all American measurements ceased. This paper briefly summarizes the chemical measurements made by SAGA 3 investigators and presents in some detail the meteorological and hydrological characteristics encountered during SAGA 3. The meteorological analysis is based on atmospheric soundings of temperature, humidity, winds, sea surface temperature, postcruise back trajectories of winds, and satellite imagery. In general, the meteorology during SAGA 3 was typical of the location and time of year. Exceptions to this include an incipient El Niño that never developed fully, a poorly defined ITCZ on 4 of 6 equator crossings, wind speeds that were 20% greater than the decadal mean, a convective event that brought midtropospheric air to the surface (on Julian day 59), and transport of northern hemispheric air to 18°S during a synoptic scale tropical disturbance.

1. EXPERIMENTAL GOALS

There is abundant evidence that trace gas emissions from industrial and agricultural activity are increasing. These trace gases are transported and modified by chemical and physical processes within the atmosphere and have resulted in demonstrable changes in the atmosphere's composition that may cause changes in the global climate. In the first half of 1990 the third Soviet-American Gases and Aerosols (SAGA 3) experiment was conducted on board the Soviet R/V *Akademik Korolev*. The primary goal of the SAGA 3 experiment was to investigate the composition of atmospheric trace gases and aerosols in the remote marine environment in order to better understand how these gases and aerosols may affect climate. In particular, studies were conducted of the seawater and atmospheric processes that produce, oxidize, modify, consume, or transport climatically active atmospheric trace species.

The SAGA 3 measurements were carried out by researchers from seven Soviet institutes and eight American institutes and are summarized in Table 1. The observations made on the SAGA 3 experiment fit into five main areas of study. The first area of study was the concentration of gases in seawater and their air-sea flux (Figure 1). Measurements were made of dissolved CO, CO_2, CH_4, and dimethyl sulfide (DMS) [*Bates et al.*, this issue], C_2-C_5 hydrocarbons [*Donahue and Prinn*, this issue; *Atlas et al.*, this issue], halocarbons [*Butler et al.*, 1991], and N_2O [*Butler et al.* 1990]. The concentration of these dissolved gases is determined by the net sum of complex biological and physical oceanic processes of production and consumption. The flux of these gases between the ocean and the atmosphere is usually assumed to be a function of the saturation gradient at the air-sea interface and wind speed. Measurements of the seawater and atmospheric concentrations of these gases were made on SAGA 3 and air-sea gas fluxes were calculated assuming an appropriate exchange velocity [*Bates et al.*, this issue]. Air-sea gas exchange was also studied by examining the saturation anomaly of the halocarbons between the surface waters and the atmosphere. Chlorofluorocarbon 11 (CFC 11) was used to study short-term physical processes (e.g., bubble injection, temperature variations, etc.) involved in air-sea exchange [*Butler et al.*, 1991]. In addition, the tropical ocean can represent a net sink of halocarbons that react with water via hydrolysis. During SAGA 3, methyl chloroform in the surface waters was found to be consistently undersaturated with respect to the atmosphere, resulting primarily from hydrolysis in seawater and perhaps some by biological destruction [*Butler et al.*, 1991].

A second area of study on the SAGA 3 cruise was photochemistry in the atmospheric marine boundary layer (MBL). The remote tropical MBL has several unique photochemical characteristics including low concentrations of NO_x and ozone [*Ridley et al.*, 1987] and high solar UV fluxes due to lower concentrations of ozone in the equatorial stratosphere (see Figure 6, *Thompson et al.* [this issue]). During SAGA 3, measurements were made of most of the key photochemical species in the MBL. These measurements

[1]NOAA Pacific Marine Environmental Laboratory, Seattle, Washington.
[2]Also at Joint Institute for the Study of Atmosphere and Ocean, University of Washington, Seattle.
[3]Institute for Applied Geophysics, Moscow, Russia.
[4]Universities Space Research Association, NASA Goddard Space Flight Center, Greenbelt, Maryland.
[5]NASA Goddard Space Flight Center, Greenbelt, Maryland.
[6]NOAA Climate Monitoring and Diagnostics Laboratory, Boulder, Colorado.

Paper number 93JD00566.
0148-0227/93/93JD-00566$05.00

TABLE 1. Chemical Measurements Made During the SAGA 3 Experiment

Species	Method	Institute	Investigator
Fluxes of Biogenic Trace Gases, Oceanic Measurements			
CO, CH_4	GC	PMEL	K. Kelly, T. Bates
CO_2	GC	PMEL	K. Kelly, T. Bates
DMS	GC, ECD-S	PMEL	J. Johnson
N_2O	GC, ECD	CMDL	J. Butler, J. Elkins
Photochemistry of the Marine Boundary Layer, Atmospheric Measurements			
CO, CH_4	GC	PMEL	K. Kelly, T. Bates
O_3	UV-Dasibi	PMEL	J. Johnson
O_3	UV-Dasibi	LAM	V. Yegorov
NO	chemiluminescence	WWF	A. Torres
NO, NO_2	chemiluminescence	LAM	V. Yegorov
H_2O_2	chemiluminescence	URI-NH	B. Mosher, B. Heikes
O_3, column	UV photometer	MGO	A. Shashkov
C_2-C_5 HCs	capillary GC	MIT	N. Donahue, R. Prinn
HCs	flask samples	NCAR	J. Greenberg, A. Thompson
Alkyl nitrates	charcoal trap	NCAR	E. Atlas, A. Thompson
Hydrocarbons, halocarbons	flask samples	NCAR	L. Heidt, A. Thompson
Organic acids	mist chamber/IC	UNH	B. Mosher
UV, for NO_2 photolysis	radiometer	GSFC	A. Thompson
Particles, Sulfur, and DMS, Atmospheric Measurements			
DMS	GC ECD-S	PMEL	J. Johnson
H_2S	filter/fluorescence	UM	S. Yvon, E. Saltzman
HNO_3, SO_2	annular denuder/IC	URI	P. Laj, B. Huebert
SO_2	filter/colorimetry	LAM	V. Yegorov
Size-resolved SO_4^{-2}, MSA	cascade impactor	URI	P. Laj, B. Huebert
SO_4^{-2}	filter	LAM	V. Yegorov
Aerosol elemental analysis	PIXE, X ray fluorescence, IR	LAM, IAP, PTI	V. Yegorov
Aerosol number Volume distribution	OPC AZ-5	IAP-PTI	B. Nazorov
Aerosol size, 0.1–1 μm	DMA	UH	J. Porter, A. Clarke
Volatile aerosol, 0.15–3 μm	LOPC, heating	UH	J. Porter, A. Clarke
CN, 0.02–1 μm	CN counter	UH	J. Porter, A. Clarke
Interhemispheric/Latitudinal Gradient of Trace Gases and Aerosols, Atmospheric Measurements			
^{85}Kr	beta-decay	MPEI	V. Novichkov
^{222}Ra	spectrometry	FHMRI, IAG	V. Koropalov
^{7}Be	spectrometry	FHMRI, IAG	V. Koropalov
^{212}Pb	spectrometry	FHMRI, IAG	V. Koropalov
Halocarbons	GC, ECD	CMDL	J. Elkins, J. Butler
Halocarbons	GC, ECD	IAG	V. Koropalov
Halons, 1211 and 1301	GC, ECD	CMDL	J. Butler, J. Elkins
N_2O	GC, ECD	CMDL	J. Elkins, J. Butler
Aerosol black carbon	aethalometer	IAP	S. Pirgov, A. Hansen
CO, CO_2, CH_4	GC	PMEL	K. Kelly, T. Bates
CO_2	GC, TCD	IAG	V. Koropalov
CO_2, total column	IR-sun photometer	MGO	A. Shashkov
CO_2	flask/NDIR	MGO	A. Shashkov
Stratospheric Aerosols			
Aerosol vertical distribution	lidar sounding	IEM	Y. Kaufman

CMDL, Climate Modeling and Diagnostics Laboratory, Boulder, Colorado; FHMRI, Far East Hydrometeorological Research Institute, Vladivostok, Russia; GSFC, Goddard Space Flight Center, Greenbelt, Maryland; IAG, Institute of Applied Geophysics, Moscow; IAP, Institute of Atmospheric Physics, Moscow; IEM, Institute of Experimental Meteorology, Obninsk, Russia; LAM, Laboratory for Atmospheric Monitoring, Moscow; MGO, Main Geophysical Observatory, St. Petersburg, Russia; MPEI, Moscow Physical Engineering Institute; MIT, Massachusetts Institute of Technology, Cambridge; PMEL, Pacific Marine Environmental Laboratory, Seattle, Washington; PTI, Physical Technical Institute, Dushanbe, Russia; UH, University of Hawaii, Honolulu; UM, University of Miami, Florida; UNH, University of New Hampshire, Durham; URI, University of Rhode Island, Naragansett; WWF, Wallops Flight Facility, Wallops Island, Virginia.

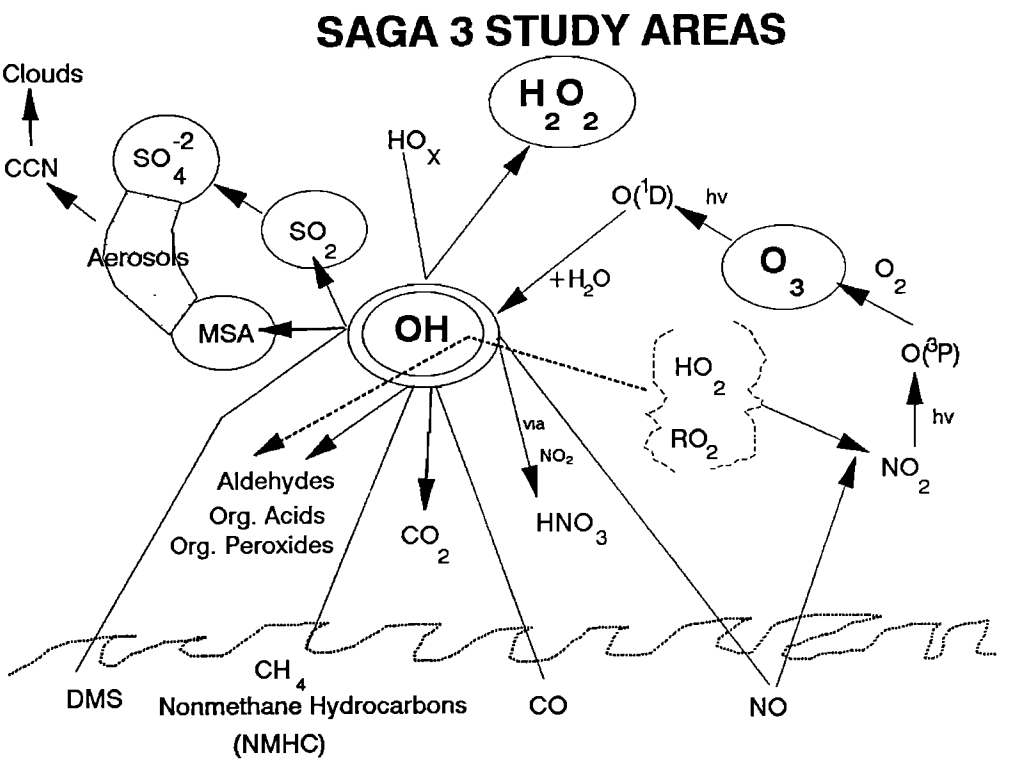

Fig. 1. Study areas.

included atmospheric NO [*Torres and Thompson*, this issue]; CO and CH_4 [Bates *et al.*, this issue]; DMS [*Huebert et al.*, this issue]; surface O_3, total column O_3, (H_2O_2), and H_2S [*Yvon et al.*, this issue]; soluble alkylperoxides and UV light [*Thompson et al.*, this issue]; C_2-C_5 hydrocarbons [*Donahue and Prinn*, this issue; *Atlas et al.*, this issue]; and alkyl nitrates [*Atlas et al.*, this issue]. Indeed, the SAGA 3 experiment appears to be the most complete set of shipboard measurements ever made of the photochemically reactive species in the remote MBL (Table 1). Numerical modeling of ambient photochemical conditions was performed using these measurements [*Thompson et al.*, this issue; *Donahue and Prinn*, this issue; *Yvon et al.*, this issue]. A primary output of the photochemical models was the evaluation of the hydroxyl radical (OH) concentration (Figure 1). From the predicted OH concentrations the atmospheric lifetimes of reduced species, DMS, and the light (C_1-C_5) hydrocarbons were calculated and compared to those deduced from seawater measurements [*Bates et al.*, this issue; *Donahue and Prinn*, this issue]. The models were also used to simulate diurnal cycles that were compared to observations of O_3 and peroxides.

A third area of study on SAGA 3 was the distribution of aerosol particles in the MBL, their physical and chemical properties, and the distribution of possible precursor gases. Most atmospheric particles have been shown to be composed primarily of sulfate which results from gas-to-particle conversion of natural and anthropogenic sulfur gases. These particles can modify climate directly by their reflection of sunlight back to space [*Shaw*, 1983; *Charlson et al.*, 1991] and indirectly via modification of optical properties of marine stratus clouds [*Charlson et al.*, 1987]. An increase in the cloud condensation nuclei (CCN) subset of these particles is calculated to result in whiter stratus clouds due to a larger number density of smaller water droplets. The sulfur source for these particles in the remote MBL is believed to be the sea-to-air flux of DMS from the sea surface. Because the biogenic production of DMS is modified by climate and because the flux of DMS can in turn modify climate, a potential climate feedback loop exists. Measurements were made of atmospheric DMS and SO_2 concentrations, size-resolved non-sea-salt sulfate and methane sulfonate concentrations [*Huebert et al.*, this issue], aerosol size distributions, size dependent aerosol volatility, and condensation nuclei [*Clarke and Porter*, this issue]. Using the aerosol volatility, the sulfate mass and the $NH_4^+/SO_4^=$ molar ratio were estimated. From these measurements, evidence was found that suggests that SO_2 is not always an intermediate in DMS oxidation and that aerosol ammonia concentration is related to the concentration of oceanic chlorophyll.

The fourth area of study was the measurement of latitudinal concentration gradients of trace species over the Pacific Ocean. Species like chlorofluorocarbons, halons, methyl chloroform, and ^{85}Kr have only anthropogenic sources. Other species, e.g., CO, CO_2, CH_4, and black carbon aerosol, have both natural and anthropogenic sources. Measurements of concentration gradients of these species were conducted on the five north-south transects of leg 1 and the two north-south transects of leg 2 [*Bates et al.*, this issue; *Elkins et al.*, 1990; *Butler et al.*, 1990, 1991]. Because the anthropogenic emissions of these gases are not at steady state and because anthropogenic emissions are mostly located in the northern hemisphere, there are concentration gradients with decreasing concentrations southward. These gradients are intensified near the equator where the intertropical convergence zone (ITCZ) forms a partial barrier to north-south mixing.

The last area of study involved stratospheric aerosol layers originating from both the constant influx of sulfur gases and the sporadic injections of volcanic SO_2. These layers were

detected with a Soviet, ship-based lidar [*Kaufman et al.*, this issue]. This project also included an intercomparison with the NOAA lidar facility at Mauna Loa Observatory during the Hilo, Hawaii, inport.

These five areas of study on SAGA 3 were not exclusive of each other in the sense that most measurements were related to more than one area of study. For example, the supply of sulfur for sulfate particles in the MBL [*Huebert et al.*, this issue] was directly related to the sea-to-air flux of biogenically produced DMS [*Bates et al.*, this issue]. The lifetime of atmospheric DMS could be calculated from the sea-to-air flux of DMS [*Bates et al.*, this issue], the atmospheric concentration of DMS [*Huebert et al.*, this issue], and the height of the MBL. The lifetime of atmospheric DMS could also be calculated using a photochemical model [*Thompson et al.*, this issue].

The large number of measurements produced a very detailed picture of the marine and atmospheric chemistry of the central equatorial Pacific. The results of these investigations are summarized in nine other papers included in this special issue.

2. Cruise Tracks and Dates

The *Akademik Korolev* departed from its home port of Vladivostok on January 28, 1991, and arrived in Hilo, Hawaii, on February 7, where the American equipment was installed. The ship left Hilo on February 12 and arrived in Pago Pago, American Samoa, on March 13, 1992, where the American equipment was removed except for that belonging to NOAA Climate Monitoring and Diagnostics Laboratory (CMDL). The *Akademik Korolev* departed Pago Pago on March 17 and arrived in Singapore on April 12 where the remaining American measurements ceased. The leg from Hilo to Pago Pago has been designated SAGA 3/leg 1 (Figure 2*a*) and the leg from Pago Pago to Singapore is referred to as SAGA 3/leg 2. Leg 1 had five north-south equator crossing transects 1 through 5. Leg 2 had one northward transect that crossed the equator (transect 6) and one southward transect that did not cross the equator (transect 7). The entire cruise track is shown in Figure 2*b*.

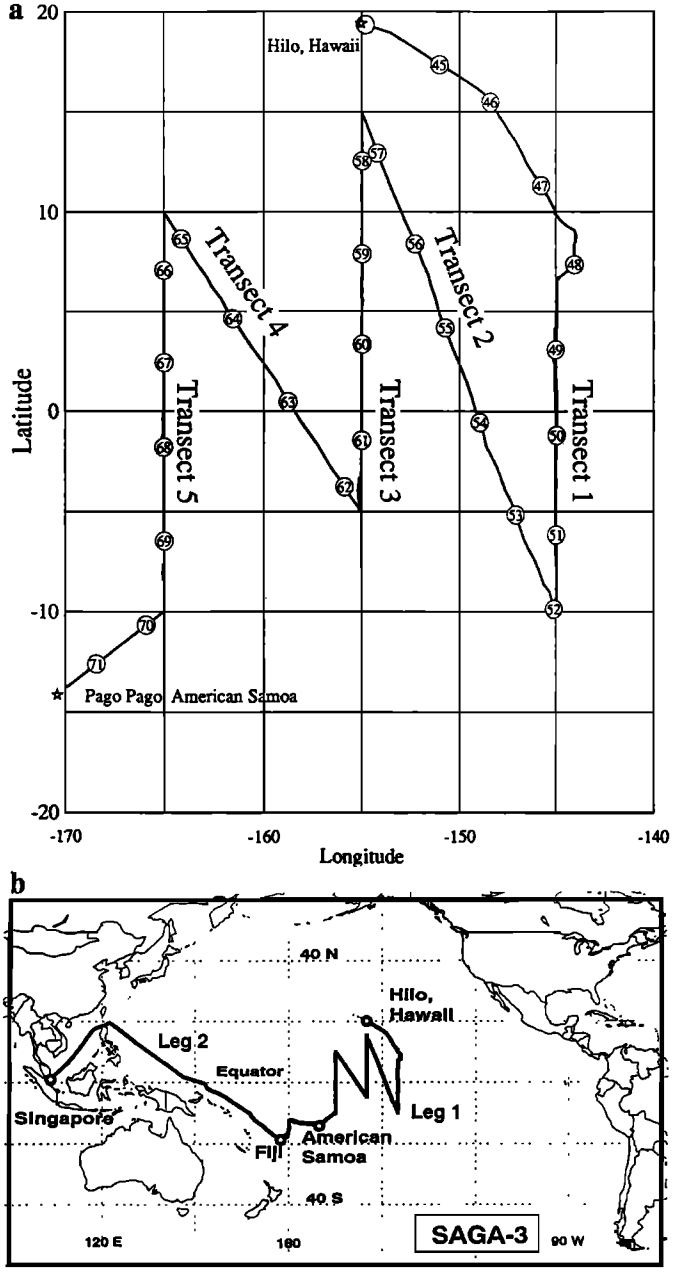

Fig. 2. (*a*) Cruise track for leg 1 of SAGA 3 (Hilo Hawaii to American Samoa). (*b*) Entire cruise track, legs 1 and 2 (American Samoa to Singapore).

3. Meteorological Overview

3.1. *Shipboard Measurements*

Shipboard measurements of standard meteorological parameters (ambient temperature, relative humidity, winds, and solar radiation) were recorded hourly during transects 1, 3, 5, and 6 and every 3 hours during transects 2, 4, and 7. These data are plotted for each transect of leg 1 as functions of latitude in Figures 3*a*–3*e* and for the two transects of leg 2 as functions of day of year in Figure 3*f* and 3*g*. Generally, temperatures increased southward along the transects. The air was quite moist, with relative humidities almost always in the range of 75 to 95%. Winds were generally from the east-northeast except during crossings of the ITCZ when the winds were much more variable. Cloudiness during ITCZ crossings is evident from the reduction of solar radiation indicated on those days.

Balloon soundings of temperature and water vapor were collected from the ship by both NOAA PMEL and Soviet investigators. The Soviet soundings were made by a traditional upper air system that had limited vertical resolution (several data points per kilometer) but were tracked by ship-based radar, so that horizontal winds were determined. The NOAA PMEL soundings gave detailed resolution (temperature, humidity, and pressure every 20 m), however, the humidity signal was lost when its wet-bulb sensor froze, limiting humidity data to altitudes less than about 5 km. The PMEL sounding system is described fully elsewhere [*Johnson and Mitchell*, 1991]. The Soviet rawinsondes were released at synoptic times (0000 and 1200 UTC) each day. The PMEL radiosondes were launched on the same balloon as the Soviet rawinsondes, but only on the three north-south transects (1, 3, and 5) were they used at all of the synoptic times.

Starting at the surface, the typical tropical marine troposphere can be divided into four major layers: the mixed layer, the cloud-containing layer, the trade wind inversion, and the free troposphere [Sarachik, 1985]. The mixed layer (ML) extends vertically from the surface, where relative humidities are typically 75–80%, to the lifting condensation level (LCL),

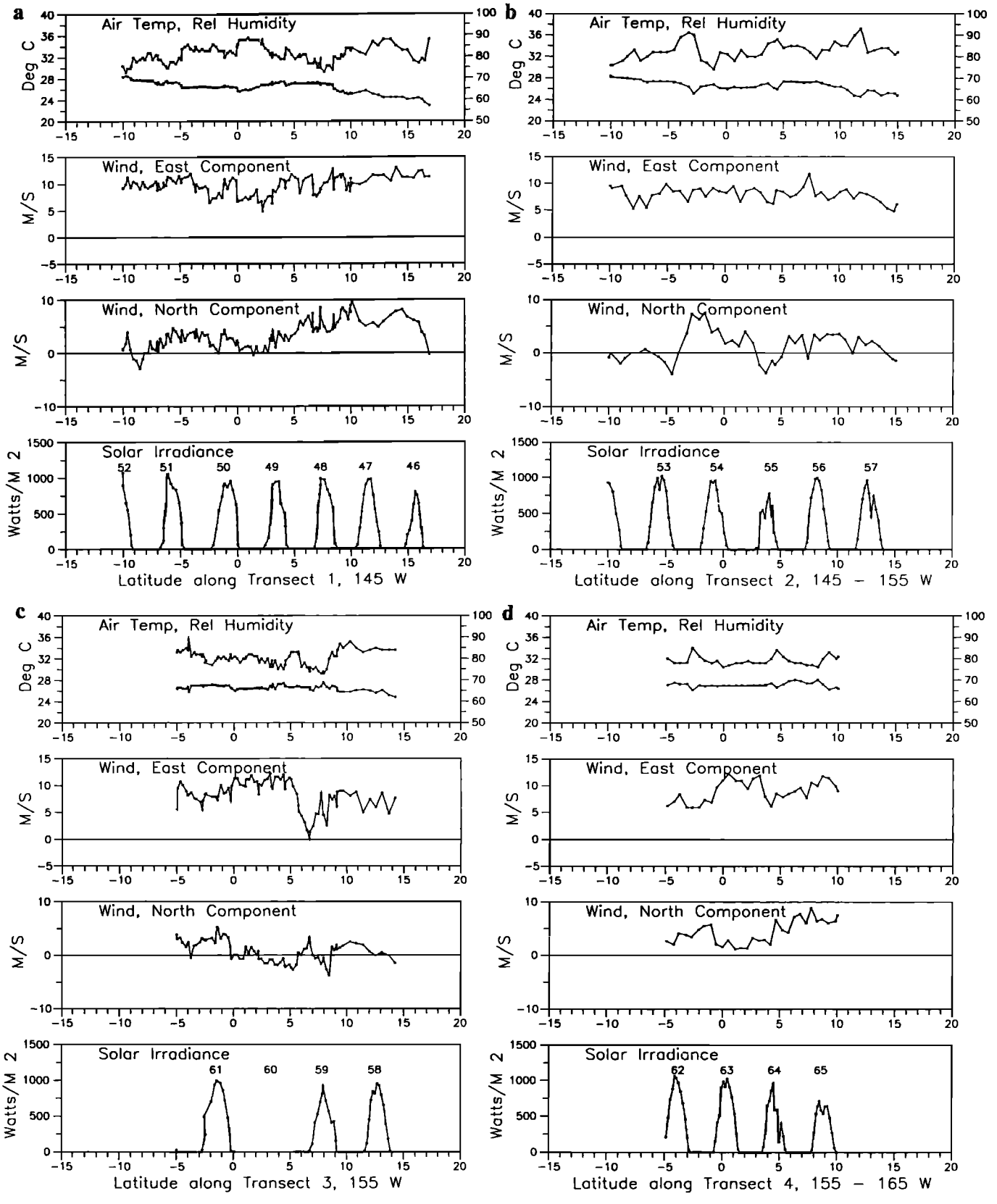

Fig. 3. Meteorological parameters measured aboard the R/V *Akademik Korolev* for each transect of leg 1. In the top panel in each of Figures 3*a*–3*g* the top curve is relative humidity and the bottom curve is air temperature. The solar irradiance was measured with a pyranometer that was located on a boom that extended 5 m in front of the bow of the ship. For leg 1 (Figures 3*a*–3*e*, transects 1–5) the position of the day of year label in the sunlight panel is the latitude of the ship at 0000 UTC on that particular day (for 3*c*, transect 3, the sunlight data on day 60 between 6.5°N and 0°N are missing.). For leg 2 (3*f* and 3*g*, transects 6 and 7) the data, including latitude, are shown as functions of day of year, and the atmospheric mixing ratio of methyl chloroform (in parts per trillion by mole fraction) is displayed instead of sunlight. The arrow indicates the period of a tropical disturbance that brought high levels of halocarbons to the southern hemisphere near Fiji.

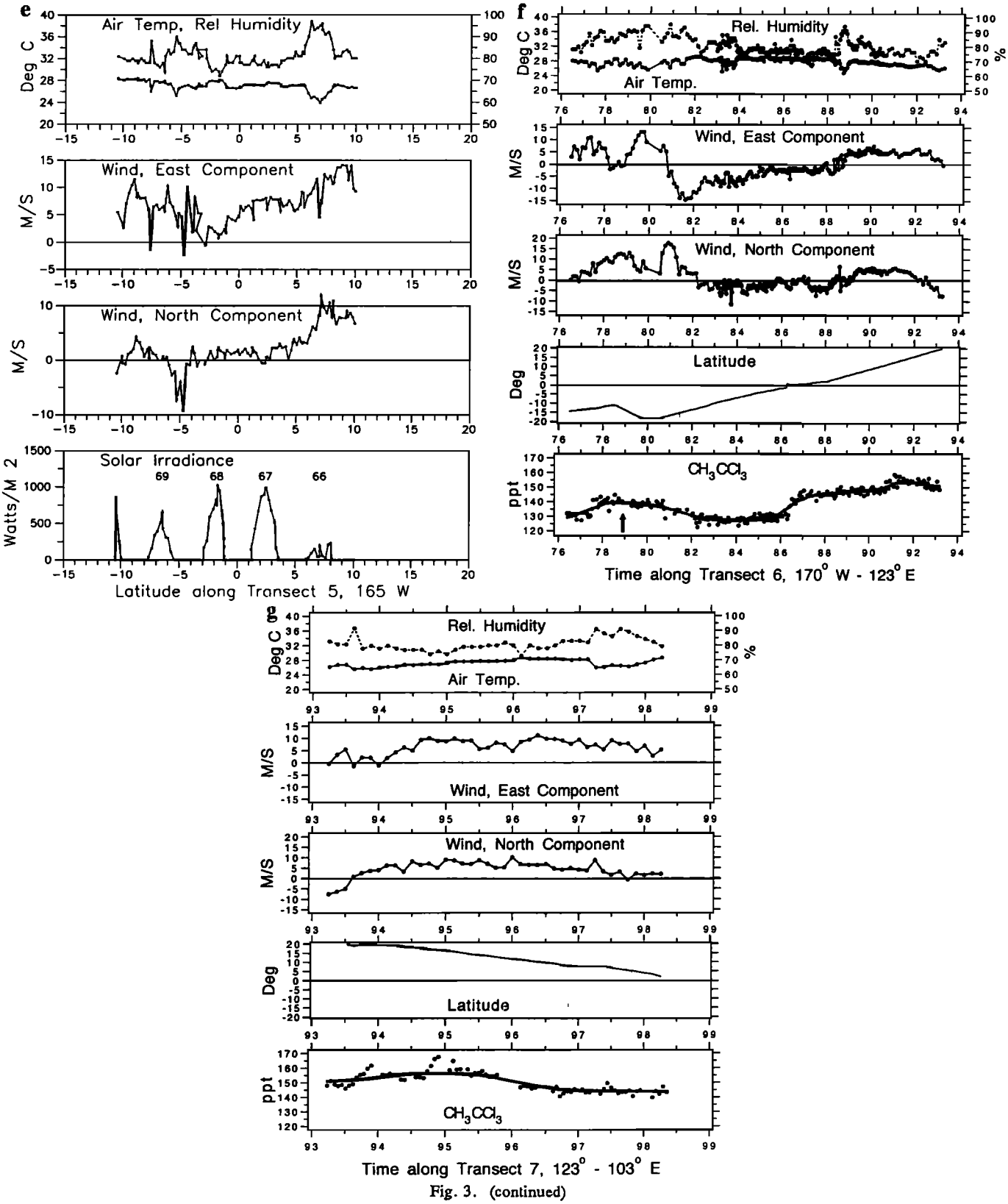

Fig. 3. (continued)

where the relative humidity is near 100%. It is characterized by rapid mixing and near-constant potential temperature and may include a superadiabatic surface layer in its lowest 100 m. The most vigorous updrafts from the mixed layer extend up into the cloud containing layer (CCL) forming isolated stratocumulus clouds. Within these clouds the relative humidity (RH) is 100%, while regions of subsidence between the clouds have an RH less than 100%. The latent heating within active clouds and the radiative cooling in the slowly subsiding air away from the clouds cause the potential temperature to increase with height within the CCL. The CCL is generally capped by the trade wind inversion (TWI), a stable layer where

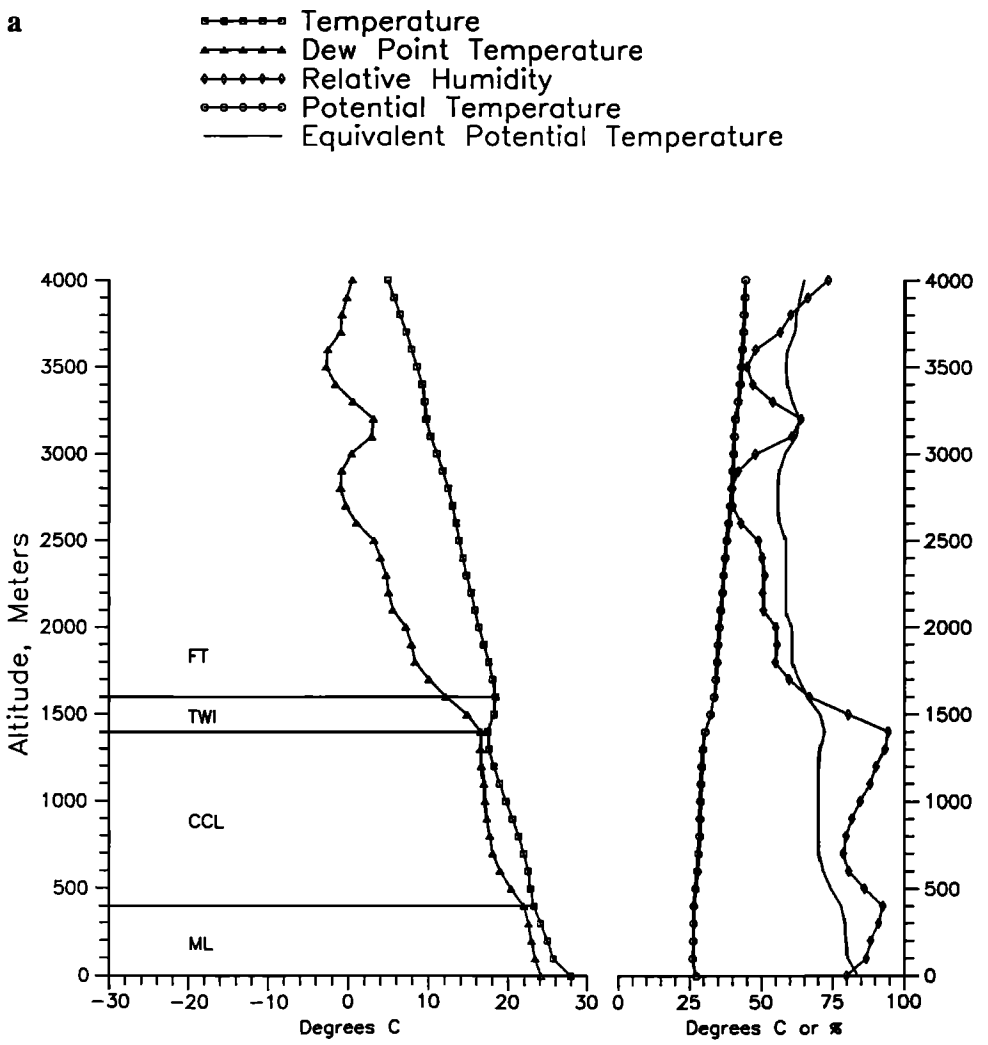

Fig. 4. (*a*) Typical atmospheric sounding from 0000 UTC on day 53, February 23, made by the Pacific Marine Environmental Laboratory (PMEL) system. The mixed layer (ML), cloud containing layer (CCL), trade wind inversion (TWI), and free troposphere (FT) are indicated. (*b*) Sounding during convective event at 0000 UTC on day 66.

both temperature and potential temperature increases with altitude for several hundred meters and the RH corresponding decreases.

Mixing within the ML is rapid, with time scales of the order of 10–20 min [*Stull*, 1988, p. 450]. The mixing within the CCL is more intermittent, since the vertical circulations are enhanced in the vicinity of active cumulus clouds occupying a small fraction of the area. Reported values for the area-averaged convective mass fluxes within the CCL [e.g., *Betts*, 1975] yield characteristic vertical velocities of ~1–4 cm s^{-1}, which imply mixing time scales of 3–12 hours. The combination of the ML and the CCL is generally considered the marine boundary layer (MBL), so the top of the CCL is also the top of the MBL. The TWI, being thermally stratified, constitutes a barrier to mixing, especially to atmospheric species having lifetimes of 1 day or less.

A typical thermodynamic profile (with the layers identified) is shown in Figure 4*a*. As with the typical sounding, all soundings revealed RH values in the MBL of greater than 75%. Above this level the dew point profile shows a decline and the relative humidity decreases substantially. The height of the top of the ML, CCL, and TWI was determined for each of the NOAA PMEL soundings and these heights are plotted in Figure 5 as a time series for the duration of leg 1. Most of the soundings showed boundary layer heights in the range 600 to 1700 m with a mean value near 1400 m. Only rarely did the height of the MBL exceed 2500 m.

In the tropics there are regions of deep intense convection where the concept of a MBL becomes meaningless. A few of our soundings were made in these convective clouds. The profile from the sounding at 0000 UTC, March 7 (Julian day 66.0), during one of these convective events, is shown as Figure 4*b* and is discussed in greater detail below.

3.2. *Large-Scale Features and Back Trajectories*

National Meteorological Center (NMC) global 1000-mbar analyses for the Pacific region were examined for the period of the cruise. Most of the period was dominated by rather featureless easterly flow. The exceptions were troughs that appeared in the northern hemisphere in the 140° to 160°W region on February 27 and 28 (days 58 and 59) and in the southern hemisphere in the 130° to 155°W region from March 6 to March 8 (days 65 to 67). Air mass trajectories on the 1000-mbar and 850-mbar surfaces were constructed using the NMC wind analyses. The trajectories were initiated at the ship's position at both 0000 and 1200 UT each day and were constructed backward in time for 10 days. Figure 6 shows a summary of the 850-mbar back trajectories arriving at the

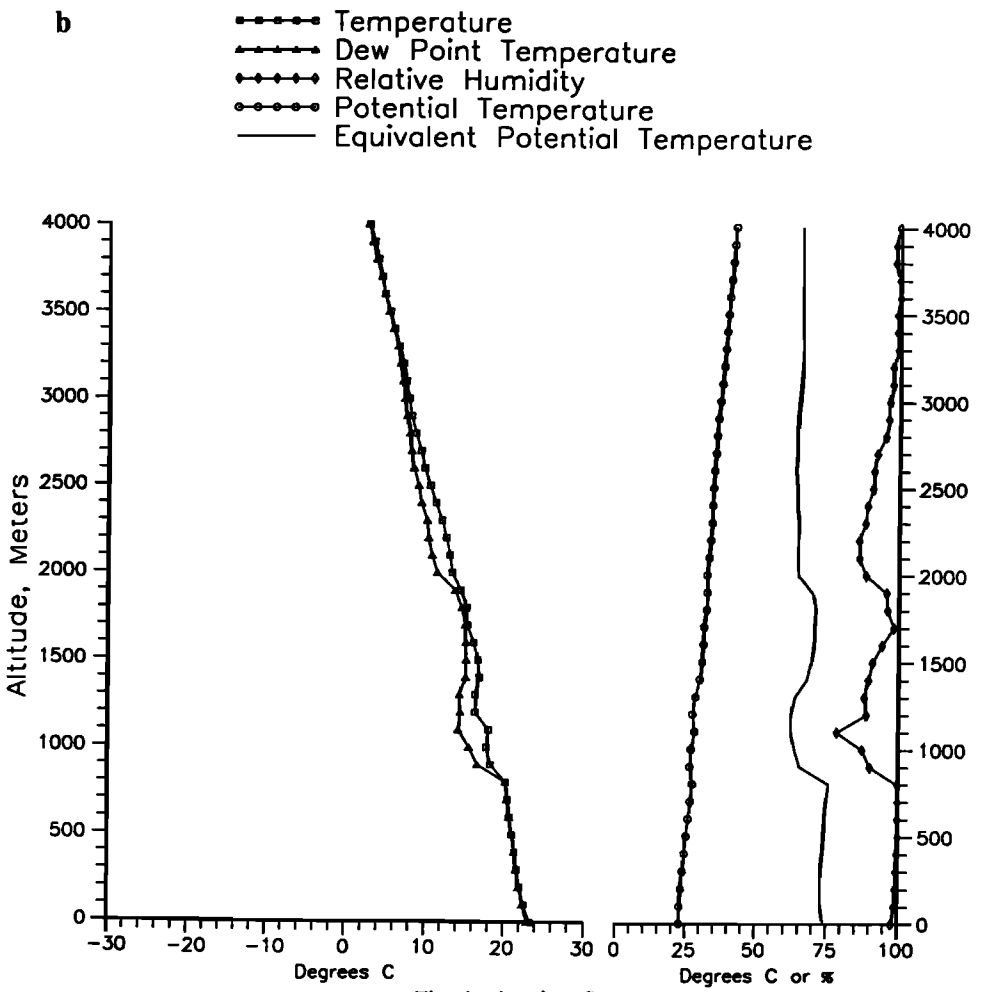

Fig. 4. (continued)

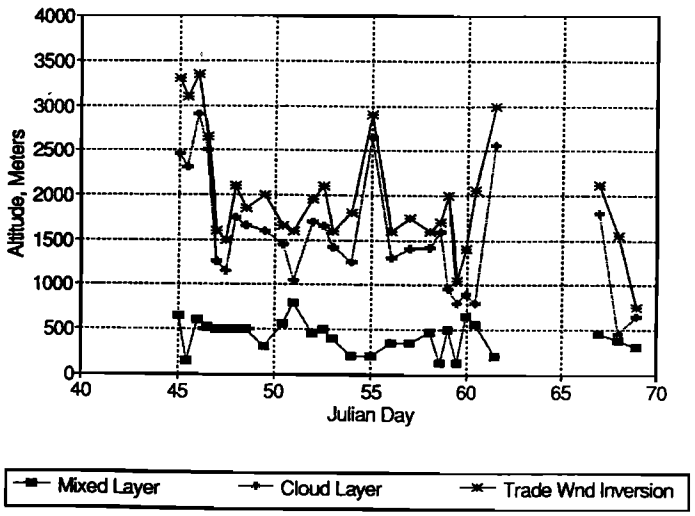

Fig. 5. Time series of the height of the top of the mixed layer, cloud-containing layer, and trade wind inversion.

cruise track at 0000 UT every second day. The 850-mbar trajectories were selected for presentation because the NMC analyses are largely based on satellite cloud-tracked winds over the remote oceans and the low-level clouds used in the analysis are more representative of the flow at 850 mbar than at 1000 mbar.

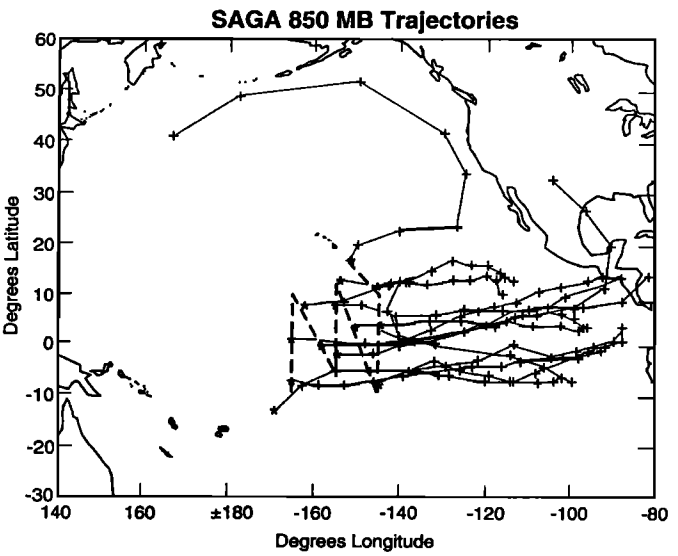

Fig. 6. The 850-mbar wind trajectories to the position of the R/V *Akademik Korolev* as calculated by Climate Modeling and Diagnostics Laboratory (CMDL). The tick marks indicate the position of a hypothetical air parcel at 12-hour intervals.

The majority of the trajectories indicate that air was arriving at the ship from the tropical eastern Pacific under generally easterly to east northeasterly flow. Therefore the history of

most of the air arriving at the ship was entirely tropical marine in nature for at least the previous 10 days. However, on four days (days 49, 59, 63, and 67) the transport speed was greater and the trajectories show the air passing over Central America and Mexico before entering the Pacific. At the beginning of leg 1 of the cruise, just southeast of the Hawaiian Islands, the origin of the air was completely different. These trajectories indicate air arriving from the middle latitudes of the northern hemisphere but still showing a completely marine history during the 10-day transport. However, given the rather large uncertainties for trajectories constructed from wind analyses over remote oceans, the possibility exists that some of the air arriving at the ship in the early part of leg 1 of the cruise could have also passed over western North America during the previous 5–10 days.

3.3. *Intertropical Convergence Zone (ITCZ) Characteristics*

Large-scale climatological analyses of the eastern tropical Pacific reveals the ITCZ as a band of confluence (usually near 5°–10°N) between the NE trades of the northern hemisphere and the SE trades of the southern hemisphere. It is important to recognize that the deep cumulus convection occurring along the ITCZ is not steady but rather is strongly modulated by westward propagating synoptic disturbances [e.g., *Chang*, 1970] with periods of about 5 days. The atmospheric conditions that are encountered during a crossing of the ITCZ therefore are controlled by one's location relative to these disturbances and by the individual characteristics of their structure. The meteorological features of each of the five crossings of the ITCZ were examined primarily with the help of GOES infrared imagery for 0000 UTC on each day of the cruise and are described below.

Transect 1 (leg 1, 145°W). There was very little evidence of the ITCZ on the first crossing other than a shift of the winds from east northeasterly to easterly. The solar radiation data (Figure 3*a*) do not indicate any major change in cloudiness at the ITCZ on this transect, verified by the GOES IR image for day 49. A summary of shipboard weather observations showed that cloud cover was actually somewhat less between 5° and 10°N than during the other segments of this transect. Most of the low clouds in both these bands were fair weather cumulus clouds. Wind speeds on this transect were strongest between 5° and 10°N.

Transect 2 (leg 1, 145°–155°W). The ITCZ was more evident on this crossing (see GOES image in Figure 7*a* for 0000 UT on day 55). Solar radiation (Figure 3*b*) was reduced to half to two thirds of the typical daytime values on days when the ship was not in the vicinity of the ITCZ. Ship weather observations also indicated the most cloudiness in the 5° to 10°N belt. Winds shifted from ENE to ESE during the ITCZ crossing and back to ENE north of the ITCZ.

Transect 3 (leg 1, 155°W). On this crossing, the ship encountered a mesoscale convective complex near the ITCZ on Julian day 59 (February 28, 1990). The solar radiation record (Figure 3*c*) does not show much of a perturbation, indicating that the ship did not encounter a widespread area of showers, as is the more typical scenario of ITCZ convection (see GOES IR image in Figure 7*b*). Instead, the ship passed through a major region of descent behind the system. The relative humidity data show a rapid drying of the air near the surface, reflecting the downward transport of drier middle tropospheric air behind the convective system. The event was followed by a gradual increase in humidity over the next 2 days. The winds showed a rapid shift from the ENE to ESE in this system, followed by a strengthening of the easterlies south of the ITCZ.

Transect 4 (leg 1, 155°–165°W). The main feature indicative of the ITCZ crossing on this transect was an increase in cloudiness on day 65. The solar radiation flux (Figure 3*d*) on this day was reduced to about two thirds of the values measured at the southern limit of this transect. The crossing also showed a shift to more northeasterly winds north of the ITCZ.

Transect 5 (leg 1, 165°W). The ship turned around in the evening of day 65 and headed south on longitude 165°W. The following day (day 66) the ship encountered the only classical ITCZ crossing of leg 1 (Figure 7*c*). The solar radiation record (Figure 3*e*) shows a daytime peak solar radiation flux reduced to about 20% of the typical value. Ship weather observations for transects 4 and 5 showed considerable cloudiness and strongest wind speeds between 5° and 10°N. Most of the low clouds in this latitude belt were cumulonimbus type clouds. During this ITCZ event the temperature was depressed approximately 3°C and the relative humidity increased from about 80% to 90 to 95%. Winds were quite strong from the northeast during the crossing, shifting to ENE and becoming weaker to the south of the ITCZ.

Transect 6 (leg 2, 172°W–123°E). While much of the photochemical instrumentation was removed in American Samoa, tracer measurements continued by Soviet and NOAA CMDL scientists. Because of a medical emergency the ship was diverted to the island of Fiji (18°S, 178°E). A synoptic scale tropical disturbance moved over the ship's track on day 77 and continued until day 80 with strong winds and heavy precipitation during the stopover in Fiji. During this period the atmospheric mixing ratios of all the halocarbons, particularly CFC 11 and methyl chloroform (Figure 3*f*), were elevated to levels observed in the northern hemisphere. Methyl chloroform increased by 10 ppt and CFC 11 by 5 ppt over the mean southern hemispheric values observed during this cruise. Analysis of infrared imagery from the GMS meteorological satellite and calculated back trajectories showed that this region of enhanced convective activity originated near the equator and the dateline and moved south to Fiji. Transport of air masses originating in the northern hemisphere with enhanced levels of methyl chloroform and CO_2 have also been observed at American Samoa, most frequently during the December to April period [*Halter et al.*, 1988]. After day 81, light winds and clear to partly clear skies prevailed for the rest of the transect. Going from south to north, an abrupt change in the mixing ratios of the halocarbons occurred at the equator similar to the interhemispheric gradient observed during transect 3 (Figure 3*f*).

Transect 7 (leg 2, 123°E–103°E). While the ship never crossed the equator during this transect, the north-south gradients of the mixing ratios of the halocarbons were similar to transects 1, 2, 4, and 5. There was no distinct ITCZ event during this transect and meteorological conditions were clear skies and light winds.

3.4. *Special Events*

Two of the transects (3 and 5, days 59 and 66) appeared to coincide with mesoscale disturbances associated with the ITCZ. However, these two disturbances were very dissimilar

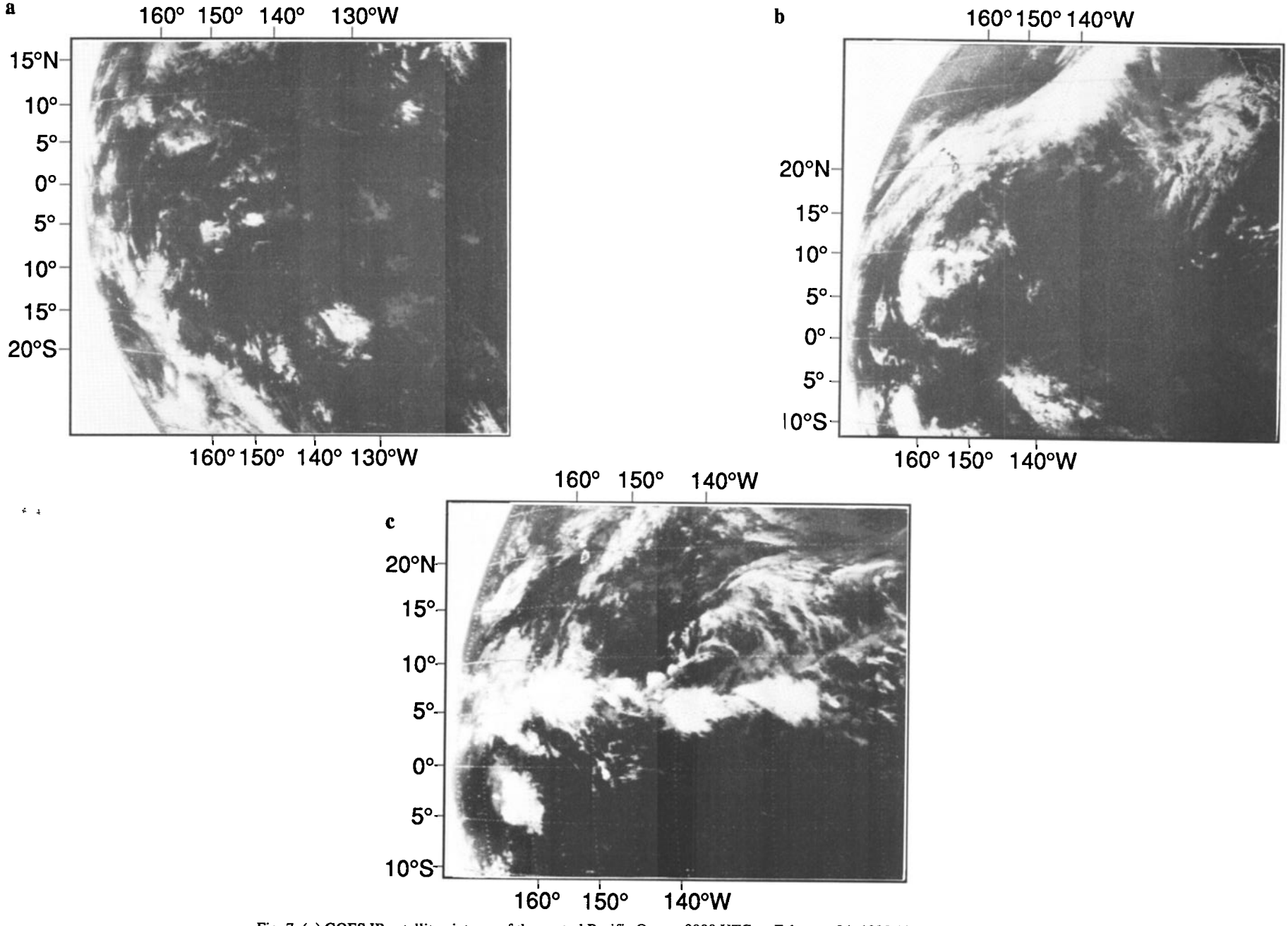

Fig. 7. (*a*) GOES IR satellite pictures of the central Pacific Ocean, 0000 UTC on February 24, 1990 (day 55); (*b*) 0000 UTC on February 28 (day 59); and (*c*) 0000 UTC on March 7 (day 66).

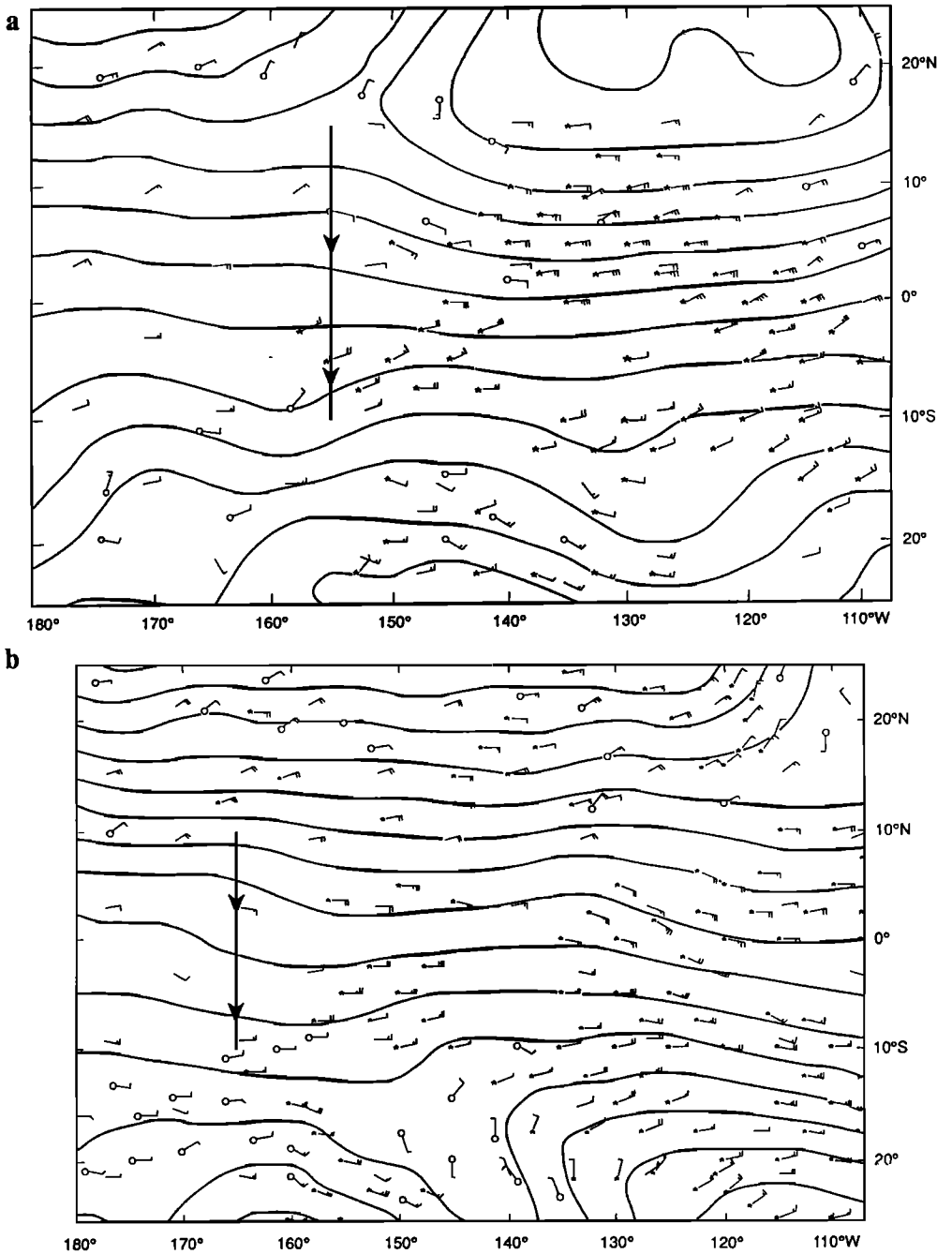

Fig. 8. National Meteorological Center (NMC) 1000-mbar streamline analysis for the tropical Pacific Ocean. (*a*) 0000 UTC on February 27 (day 58); and (*b*) 0000 UTC on March 6 (day 65).

in their meteorological and photochemical characteristics. Our purpose here is to more fully examine some of the differences between the weather encountered on day 59 of transect 3 with that on day 66 of transect 5.

Day 59. The GOES IR image for this date (Figure 7*b*) shows that the ship steamed behind an isolated, organized convective complex or system extending from about 3°N to 12°N and from about 160°W to 148°W. It appears there was a N-to-S-oriented line of vigorous convection at its leading (western) edge with a more patchy distribution of stratiform and cumuliform clouds trailing to the east. Its northern portion appears to be influenced by the extratropical storm system farther north. Additional satellite imagery (not shown) suggests that the mature phase of this convective system lasted about half a day from 1600 UTC on day 58 to 0200 UTC on day 59. After the latter time the system was primarily composed of a loose stratiform region that gradually dissipated as the ship steamed southward. The ship encountered stratiform rain for several hours between 8° and 4°N (2100 UTC on day 58 to 1700 UTC on day 59.) The presence of this system is only barely indicated by the 1000-mbar analysis for 0000 UTC, February 28, 1990, from NMC (Figure 8*a*), which shows only a slight cyclonic curvature of the streamlines near the ship's location at about 8°N, 155°W. The soundings from the ship, however, reveal tropospheric structures that probably reflect the presence of the system, and these structures were unlike those found during the other ITCZ transects of SAGA 3.

Figure 9 illustrates the upper air characteristics during transect 3, and, in particular, during the time period of the day 59 (February 28) squall line. The plots in Figure 9 were

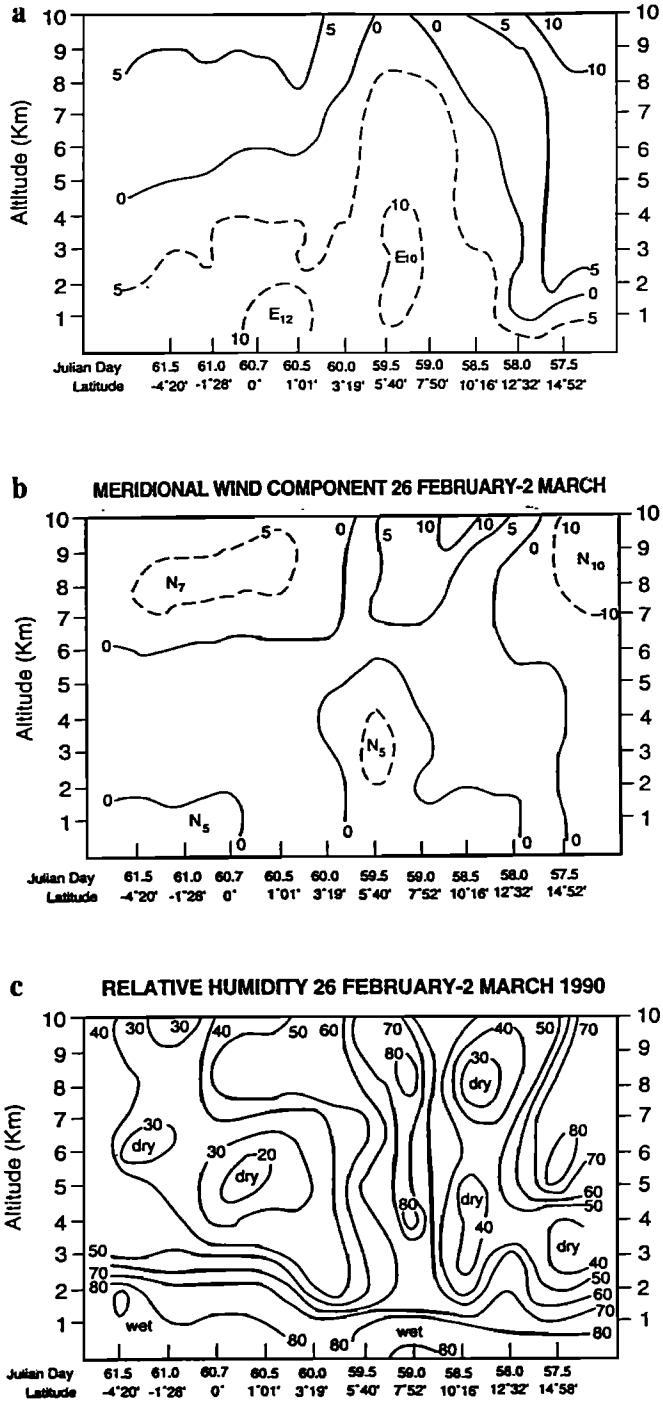

Fig. 9. Height-time (also height-latitude) cross sections from the Soviet rawinsonde system for transect 3 of (*a*) zonal winds (in m s^{-1}); (*b*) meridional winds (in m s^{-1}); and (*c*) relative humidity (in percent).

constructed from the 0000 UT and 1200 UT Soviet balloon soundings taken from the ship as it progressed southward along 155°W. The easterlies (Figure 9*a*) were found only up to 2 km on the 2 days prior to the squall event, but they were found at much higher altitudes as the ship progressed southward, reaching 9 km on day 59. The northerly component of the wind intensified on day 59, with a northerly component evident up to 5 km. The divergence in the north-south component of the wind implied by Figure 9*b* is weak below about 2 km; significant divergence is indicated from about 2 km to 4 km between 6°N and 10°N. The sounding at 7°52'N exhibits a local minima in relative humidity (Figure 9*c*) near 2–3 km. Relatively low humidities (less than 80%) were also measured at the surface by the ship between about 8° and 6°N (Figure 3*c*).

The satellite imagery and surface and upper air data from the ship suggest that the convective system of day 59 resembles the tropical squall lines analyzed by *Zipser* [1977] or the tropical mesoscale convective system (TMCS) shown by *Balsley et al.* [1991]. The latter analysis was based on wind profiler measurements from Christmas Island at 2°N, 157°W, very near the location of the disturbance on day 59. Both studies featured mesoscale midlevel (about 3 to 5 km) downdrafts behind the leading line of strong upward motion. *Zipser* [1977] indicated that the air within these downdrafts can originate ahead of or behind the main updraft. He also indicates that this downdraft is relatively dry. *Balsley et al.* [1991] show enhanced easterlies between about 4 and 10 km behind this downdraft. All of these results are consistent with the observed structure on day 59. It should be noted that the ship did not pass through the band of deep, vigorous cumulus convection that was present at the leading edge of the system.

The passage of the squall line had a significant effect on trace gas mixing ratios recorded on board the ship, as described by *Thompson et al.* [this issue]. For example, behind the squall line, shipboard O_3 mixing ratios more than doubled, rising to over 20 parts per billion by volume (ppbv). We believe that these higher mixing ratios originated from downward transport of middle tropospheric air containing greater amounts of O_3 than are normally found at the surface.

Day 66. The ship's weather observations on day 66 show heavy rain for a sustained period of 6 hours. During all of leg 1 all other events of heavy precipitation lasted for at most 3 hours.

The GOES IR image for 0000 UTC, March 7, 1990 (Figure 7*c*), shows a band of enhanced cloudiness between about 5°N and 8°N extending from about 125°W to at least about 175°W. The deep convection along the ITCZ was therefore much more extensive on day 66 than on day 59, when only a single, localized convective system was evident in the region. The ship's track along 165°W was underneath the central portion of a cloud cluster spanning about 1000 (500) km in the zonal (meridional) direction. The NMC 1000-mbar analysis for 0000 UTC, March 7, 1990 (Figure 8*b*), shows easterly to southeasterly winds ranging from 7 and 12 m s^{-1} between 120°W and 170°W and 5°N and the equator and northeasterly to easterly winds of about 10 m s^{-1} for the same range of longitudes along 10°N. This suggests that there was a long E-to-W-oriented band of low-level convergence on day 66, as opposed to a localized N-to-S-oriented line of convergence and deep convection on day 59.

Figure 10 contains time/height sections similar to those in Figure 9 but for along the 165°W transect. These plots illustrate the upper air conditions of the ITCZ crossing on day 66. During this period the easterlies were found up to about 5 km and winds with a northerly component were evident as high as 2–3 km. The north-south component of the wind (from the soundings shown in Figure 10*b* and the surface data shown in Figure 3*e*) exhibited substantial convergence below 1.5 km between about 8°N and 5°N. Moist conditions up to 10 km during the ITCZ crossing are evident in the sounding at 0000 UTC, day 66 (Figures 10*c* and 4*b*), which was released directly into a convective cloud. In summary, the wind and relative

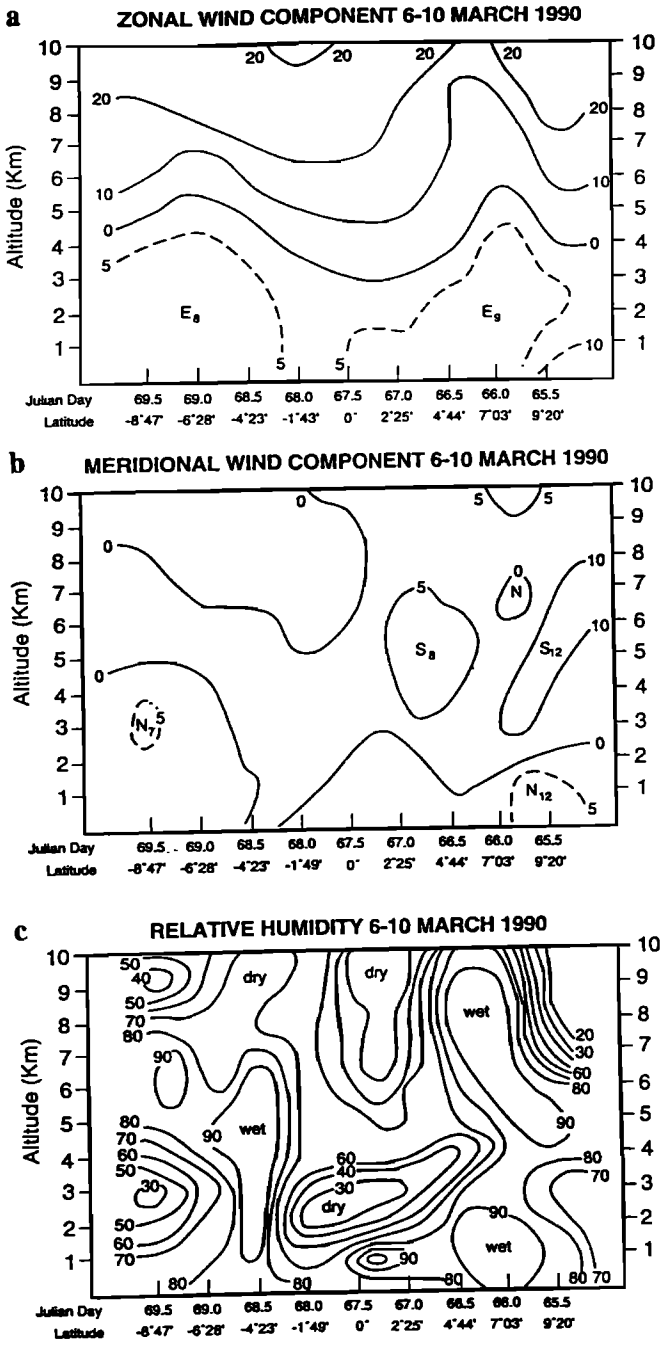

Fig. 10. As in Figure 9 but for transect 5.

humidity observations on day 66 suggest that the ship was located underneath a region of ascent.

The effects on trace gas mixing ratios were not at all similar to those that occurred on day 59. The convection on day 66 was apparently not as effective in transporting lower water vapor mixing ratios and higher O_3 mixing ratios downward from the middle troposphere, as was the squall line of day 59.

4. Oceanographic Conditions and Climatological Anomalies

4.1. *El Niño Southern Oscillation (ENSO) and Large-Scale Climatology*

Most climatological anomalies in the tropical Pacific Ocean are directly related to El Niño Southern Oscillation (ENSO) events. During "normal" conditions the easterly (westward flowing) trade winds induce a westward flowing oceanic current at the equator. This westward flowing current results in upwelling at the equator with relatively cooler water in the eastern tropical Pacific Ocean and relatively warmer water in the western tropical Pacific Ocean. The east-to-west temperature gradient in turn induces a west-to-east pressure gradient that helps to maintain the easterly trade winds. During ENSO events all of these features lessen or reverse.

A plot of the Southern Oscillation index (SIO) (the normalized difference in sea level pressure between Tahiti and Darwin, Australia) is shown in Figure 11. Although the SIO became negative, most dramatically so in February, the event was very short-lived and returned to near zero by April, implying that a full-fledged El Niño did not develop. An analysis of the sea surface temperatures for the region bounded by 140°W, 170°W, 5°N, and 5°S shows that the departure of the seasonal sea surface temperature (SST) from its mean during February and March 1990 was less then 0.5°C (*Climate Diagnostics Bulletin*, February 1990 and March 1990) with only very small positive anomalies in the eastern part of the cruise region and small negative anomalies in the western part. SST measurements from the ship (Figure 12) showed that there was a minimum at the equator of about 1°, during transects 1, 2, and 3 (145°, 150°, and 155°W) but that on transect 5 (165°W) there was no detectable SST minimum at the equator.

Other climatological information for February 1990 (*Climate Diagnostics Bulletin*, February 1990) includes the NMC 850-mbar zonal wind anomaly for 5°N to 5°S and the anomaly of outgoing longwave radiation. The 850-mbar zonal winds were very close to normal, with anomalies <1 m s^{-1}. The outgoing longwave radiation anomaly was as much as 10 W m^{-2} lower than normal, indicating some enhancement of deep convective activity over the region.

4.2. *Biological Properties*

In the central tropical Pacific Ocean, many of the biological processes are nutrient-limited [*Barber and Chavez*, 1991]. The upwelling of water from below the oceanic mixed layers brings fresh nutrients that stimulates primary productivity. Thus during "normal" conditions the equatorial Pacific Ocean is a rich biological zone with relatively high primary productivity. During ENSO events the decline in equatorial upwelling lowers productivity and so, presumably, the oceanic production of biogenic gases. Although equatorial upwelling was somewhat diminished during SAGA 3, it was nonetheless evident, so that biological productivity, while not so great as could be expected during negative temperature anomalies, was likely characteristic of this region during this season.

One indicator of upwelling is the partial pressure of dissolved N_2O in surface waters [*Elkins et al.*, 1978]. While equatorial upwelling and higher levels of dissolved N_2O were observed during leg 1, dissolved N_2O was near saturation at all times during leg 2, similar to previous measurements made in the western Pacific Ocean during SAGA 2 which occurred during an ENSO event [*Butler et al.*, 1989].

4.3. *Wind Speed and Air-Sea Flux*

A number of projects during SAGA 3 involved various aspects of air-sea transfer of trace gases. Most current theories of air-sea gas transfer [*Liss and Merlivat*, 1986; *Smethie et al.*, 1985; *Wanninkhof*, 1992] use a transfer coefficient that is

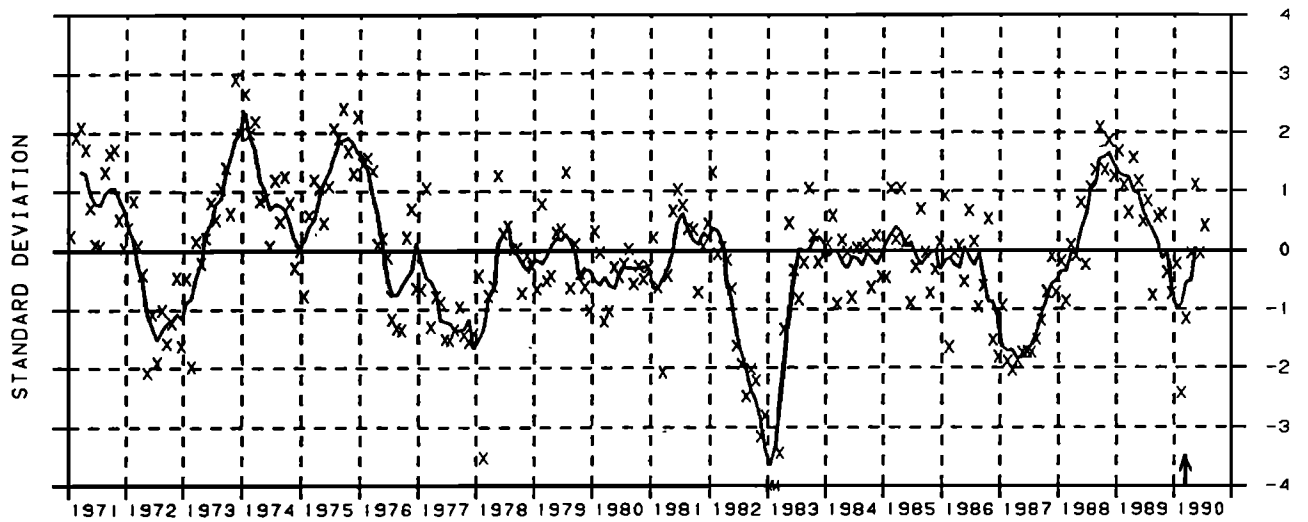

Fig. 11. The Southern Oscillation index (SOI), the difference in atmospheric sea level pressure between Tahiti and Darwin, normalized to one standard deviation, plotted from 1971 to mid-1990. The solid curve is a 5-month running mean and the crosses are individual monthly means. (Taken from *Climate Diagnostics Bulletin*, July 1990.) The time of the SAGA 3 experiment is indicated with an arrow.

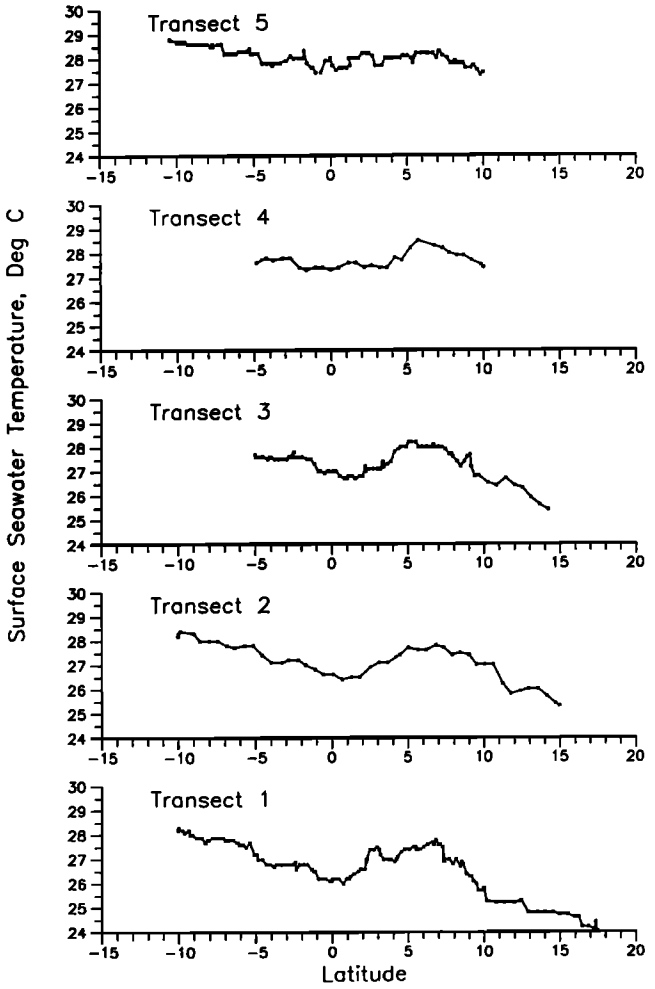

Fig. 12. Sea surface temperature measurements from the *Akademik Korolev* for each of the five transects of leg 1 plotted as functions of latitude.

strongly dependent on wind speed. Air-sea transfer rates occurring during the SAGA 3 experiment can only be considered typical if the wind speed encountered during the experiment were typical. We thus compared the wind speeds encountered during SAGA 3 to a climatological mean.

Wind speed observations from the *Akademik Korolev* (hourly during transects 1, 3, and 5 of leg 1 and every 3 hours at all other times) were compared to a 10-year record of winds from moored buoys, maintained by PMEL, and located on 140°W at 9°, 7°, 5°, 2°, and 0°N and 2°, 5°, and 7°S. The wind speeds measured by the ship at a height of 23 m and by the buoys at a height of 3 m were corrected to a common height of 10 m assuming a logarithmic wind profile (Monin-Obukhov similarity) and the drag coefficient suggested by *Large and Pond* [1982]. These corrections increase the buoy wind speeds by ~14% and decrease the ship's wind speeds by ~8%. The ship winds had a mean (10 m in altitude) value of 8.2 m s^{-1} with a standard deviation of 2.8 m s^{-1}, and the buoy record had a corresponding mean and standard deviations of 7.0 ± 2.0 m s^{-1}. A histogram of the ship wind speed observations is shown in Figure 13*a* and the buoy wind speeds in Figure 13*b*. This simple exercise shows that the mean wind speed encountered during SAGA 3 was 20% above the climatological mean, with corresponding higher air-sea transfer rates.

5. Summary

The meteorological and oceanographic conditions encountered during the SAGA 3 project were generally representative of conditions usually found in the central Pacific Ocean. Although it appeared that an El Niño was beginning to develop, with the SIO becoming negative during February, the event was very short-lived and returned to near zero by April, so that a full-fledged El Niño did not develop. The winds encountered along leg 1 were fairly typical with almost all back trajectories arriving from the east or east northeast. The wind speeds were some 20% higher than the climatological mean, likely causing a corresponding increase in the rate of air-sea fluxes of trace gases. A sharp ITCZ was only found on one of the five equator crossings (transect 5) of leg 1 and possibly during the one equatorial transect of leg 2. Atmospheric halocarbons appear to be excellent tracers of large-scale meteorological events involving north-south exchange of air masses.

The SAGA 3 project produced one of the most complete sets of atmospheric chemistry measurements in the remote marine boundary layer. As expected, the variance in the atmospheric

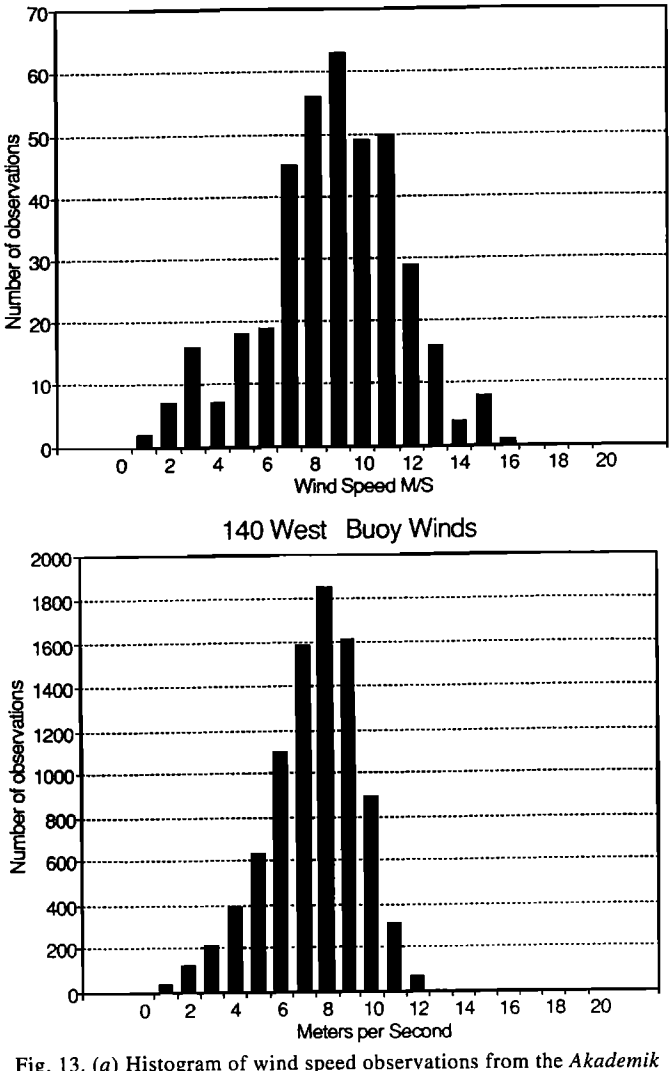

Fig. 13. (*a*) Histogram of wind speed observations from the *Akademik Korolev* (hourly on transects 1, 3, and 5, every 3 hours on transects 2 and 4) corrected to a height of 10 m. (*b*) Histogram of daily mean wind speed observations from buoys on 140°W (at 9°, 7°, 5°, 2°, and 0°N and 2°, 5°, and 7°S) during the past 10 years corrected to a height of 10 m.

concentrations of most longer-lived species was dominated by south-to-north gradients [*Butler et al.*, 1991; *Bates et al.*, this issue], or by convective events that occurred on transects 3 and 5 [*Thompson et al.*, this issue]. By measuring NO, CO, O_3, CH_4, H_2O, and NMHC, a complete photochemical model was constructed with a prediction of the crucial specie, the OH radical. One critical test of the measurements and the model is the ability of the model to duplicate the measured diurnal cycles of O_3, H_2O_2, and alkyperoxides. The sulfur gas and aerosol measurements revealed that our understanding of the sulfur cycle is still incomplete. In particular, evidence was found that suggests that SO_2 in not always an intermediate in DMS oxidation [*Huebert et al.*, this issue].

Acknowledgments. We appreciate the support of the officers and crew of the *Akademik Korolev*. SAGA 3 was a project of Working Group VIII of the U.S.-USSR Environmental Bilateral Agreement which has been coordinated in the United States by the NOAA National Climate Program Office (NCPO). Robert Etkins and Renee Tatusko of NCPO did invaluable work in clearing the many bureaucratic hurdles of international politics encountered in bringing a Soviet ship into U.S. waters. Nancy Soreide of PMEL provided the buoy wind data. Joyce Harris and Gary Herbert of NOAA CMDL determined wind back trajectories. We thank Elmer Robinson and Judy Pereira of the NOAA CMDL Mauna Loa Observatory and M. Emily Wilson-Godinet of the NOAA CMDL American Samoa Observatory for helping with equipment logistics and personnel issues. This work was carried out under the radiatively important trace species (RITS) and the marine sulfur and climate components of the NOAA Climate and Global Change Program. This is contribution 1373 from the NOAA Pacific Marine Environmental Laboratory and contribution 186 from the Joint Institute for the Study of the Atmosphere and Ocean.

REFERENCES

Atlas, E., W. Pollock, J. Greenberg, L. Heidt, and A. Thompson, Alkyl nitrates, nonmethane hydrocarbons, and halocarbon gases over the equatorial Pacific Ocean during SAGA 3, *J. Geophys. Res.*, this issue.

Balsley, B. B., D. A. Carter, A. C. Riddle, W. L. Ecklund, and K. S. Gage, On the potential of VHF wind profilers for studying convective processes in the tropic, *Bull. Am. Meteorol. Soc., 72*, 1355–1360, 1991.

Barber, R. T., and F. P. Chavez, Regulation of primary productivity rate in the equatorial Pacific, *Limnol. Oceanogr., 36*, 1803–1815, 1991.

Bates, T. S., K. C. Kelly, and J. E. Johnson, Concentrations and fluxes of dissolved biogenic gases (DMS, CH_4, CO, CO_2) in the equatorial Pacific during the SAGA 3 experiment, *J. Geophys. Res.*, this issue.

Betts, A. K., Parametric interpretation of trade-wind cumulus budget studies, *J. Atmos. Sci., 32*, 1934–1945, 1975.

Butler, J. H., J. W. Elkins, T. M. Thompson, and K. B. Egan, Tropospheric and dissolved N_2O of the West Pacific and East Indian oceans during the El Niño Southern Oscillation event of 1987, *J. Geophys. Res., 94*, 14,865–14,878, 1989.

Butler, J. H., J. W. Elkins, B. D. Hall, T. H. Swanson, T. M Thompson, and V. Koropalov, Reflections of surface-ocean trace gas concentrations in the atmospheric boundary layer: Implication for air-sea exchange and atmospheric transport, *Eos Trans. AGU, 71*, 1226, 1990.

Butler, J. H., J. W. Elkins, T. M. Thompson, B. D. Hall, T. H. Swanson, and V. K. Koropalov, Oceanic consumption of CH_3CCl_3: Implications for tropospheric OH, *J. Geophys. Res., 96*, 22,347–22,356, 1991.

Chang, C. P., Westward propagating cloud patterns in the tropical Pacific as seen from time composite satellite photographs. *J. Atmos. Sci., 27*, 133–138, 1970.

Charlson, R. J., J. E. Lovelock, M. O. Andreae, and S. G. Warren, Oceanic phytoplankton, atmospheric sulfur, cloud albedo, and climate, *Nature, 326*, 655–661, 1987.

Charlson, R. J., J. Langner, H. Rodhe, C. B. Leovy, and S. G. Warren, Perturbation of the Northern Hemisphere radiative balance by backscattering from anthropogenic aerosols, *Tellus, 43*(AB), 152–163, 1991.

Clarke, A. D., and J. N. Porter, Pacific marine aerosol II, Equatorial gradients in chlorophyll, ammonium, and excess sulfate during SAGA 3, *J. Geophys. Res.*, this issue.

Donahue, N. M., and R. G. Prinn, In situ nonmethane hydrocarbon measurements on SAGA 3, *J. Geophys. Res.*, this issue.

Elkins, J. W., S. C. Wofsy, M. B. McElroy, C. E. Kolb, and W. A. Kaplan, Aquatic sources and sinks for nitrous oxide, *Nature, 275*, 602–606, 1978.

Elkins, J. W., J. H. Butler, B. D. Hall, T. Swanson, J. Harris and G. Herbert, Measurements of atmospheric halocarbons during SAGA 3: Analysis of trajectories, meteorology and comparison with other long-lived species, *Eos Trans. AGU, 71*, 1229, 1990.

Halter, B. C., J. M. Harris, and T. J. Conway, Component signals in the record of atmospheric carbon dioxide concentration at American Samoa, *J. Geophys. Res., 93*, 15,914–15,918, 1988.

Huebert, B. J., S. Howell, P. Laj, J. E. Johnson, T. S. Bates, P. K. Quinn, V. Yegorov, A. D. Clarke, and J. N. Porter, Observations of the atmospheric sulfur cycle on SAGA 3, *J. Geophys. Res.*, this issue.

Johnson, J. E., and W. Mitchell, Structure of the marine boundary layer over the Pacific Ocean during the RITS 88 and RITS 89 cruises, *NOAA Data Rep., ERL PMEL-27*, 105 pp., Natl. Oceanic and Atmos. Admin., Boulder, Colo., 1991.

Kauffman, Y. G., S. S. Khmelevtsov, and T. E. DeFoor, Lidar measurements of stratospheric aerosols during the SAGA 3 expedition, *J. Geophys. Res.*, this issue.

Large, W. A., and S. Pond, Sensible and latent heat measurements over the ocean, *J. Phys. Oceanogr., 12*, 464–482, 1982.

Liss, P. S., and L. Merlivat, Air-sea gas exchange rates: Introduction and synthesis, in *The Role of Air-Sea Exchange in Geochemical Cycling*, edited by P. Buat-Menard, pp. 113–127, D. Reidel, Norwell, Mass., 1986.

Ridley, B. A., M. A. Carroll, and G. L. Gregory, Measurements of nitric oxide in the boundary layer and free troposphere over the Pacific Ocean, *J. Geophys. Res., 92*, 2025–2048, 1987.

Sarachik, E. S., A simple theory for the vertical structure of the tropical atmosphere, *Pure App. Geophys.*, 123, 261–271, 1985.

Shaw, G. E., Bio-controlled thermostasis involving the sulfur cycle, *Clim. Change, 5*, 297–303, 1983.

Smethie, W. M., Jr., T. Takahashi, D. W. Chipman, and J. R. Ledwell, Gas exchange and CO_2 flux in the tropical Atlantic Ocean determined from $_{222}Rn$ and pCO_2 measurements, *J. Geophys. Res., 90*, 7005–7022, 1985.

Stull, R. B., An introduction to boundary layer meteorology, 666 pp., Kluwer Academic, Hingham, Mass., 1988.

Thompson, A. M., et al., SAGA 3 ozone observations and a photochemical model analysis of the marine boundary layer during SAGA 3, *J. Geophys. Res.*, this issue.

Torres, A. L., and A. M. Thompson, Nitric oxide in the equatorial Pacific boundary layer: SAGA 3 measurements, *J. Geophys. Res.*, this issue.

Yvon, S. A., D. J. Cooper, V. Koropalov, and E. S. Saltzman, Atmospheric hydrogen sulfide over the equatorial Pacific (SAGA 3), *J. Geophys. Res.*, this issue.

Wanninkhof, R. H., Relationship between wind speed and gas exchange over the ocean, *J. Geophys. Res., 97*, 7373–7382, 1992.

Zipser, E. J., Mesoscale and convective-scale downdrafts as distinct components of squall-line structure, *Mon. Weather Rev., 105*, 1568–1589, 1977.

N. Bond and J. E. Johnson, NOAA Pacific Marine Environmental Laboratory, 7600 Sand Point Way NE, Seattle, WA 98115.

J. W. Elkins, NOAA Climate Monitoring and Diagnostics Laboratory, 325 Broadway, Boulder, CO 80303.

V. M. Koropalov, Institute for Applied Geophysics, Moscow, Russia.

K. E. Pickering, Universities Space Research Association, NASA Goddard Space Flight Center, Greenbelt, MD 20771.

A. M. Thompson, NASA Goddard Space Flight Center, Code 916, Greenbelt, MD 20771.

(Received August 31, 1992;
revised March 1, 1993;
accepted March 3, 1993.)